Ozone Induced Surface Climate Change

Yongyun Hu[1,2*], Ka-Kit Tung[2], Drew T. Shindell[1] and Gavin A. Schmidt[1]

[1]*NASA Goddard Institute for Space Studies*

and Center for Climate Systems Research

Columbia University

2880 Broadway, 112th Street

New York, NY 10025

[2]*Department of Applied Mathematics*

University of Washington

P.O. Box 352420

Seattle, WA 98195-2420

[*]*To whom correspondence should be addressed. E-mail: yhu@giss.nasa.gov*

(October 24, 2002)

Submitted to *Sciences*

Based on observational data analysis and general circulation model (GCM) simulations, we suggest that ozone depletion in the stratospheric Arctic plays the major role in causing late winter and springtime warming over the high-latitude Northern-Hemisphere (NH) continents during the past two decades. Our results show that during late winter and springtime stratospheric temperature contrasts between the Arctic and middle latitudes have been significantly enhanced since 1979. This is consistent with the observed downward ozone trend. The enhanced temperature gradients lead to strengthened westerly winds near the stratospheric subpolar region, which refract planetary wave toward low latitudes and reduce wave activity at high latitudes in both the stratosphere and the troposphere. This enhances the prevailing westerly winds over the high-latitude surface, which blow warm and moist air from oceans to the continents and cause late winter and springtime warming over the continents.

Observations show that winter and springtime (January-February-March, JFM) surface air temperatures (SAT) over the high-latitude NH continents has a warming trend since 1980s (1, 2, 3). It has been proposed that this is a signal of global greenhouse warming (1). Recent climate studies found that such a regional warming is related to a dynamical phenomenon, the so-called NH Annular Mode (NAM) or Arctic Oscillation (AO), and that the warming trend is consistent with the positive trend in the NAM index (3, 6). These studies further pointed out that when the NAM evolves toward its high-index polarity, westerly winds over the high-latitude surface become more prevailing, which blow warm and moist air from the North Atlantic and Pacific to the continents and lead to high-latitude warming. A fundamental question then emerges: what caused the positive trend in the NAM index and associated high-latitude surface warming? In this study, we shall present evidence that the surface warming is likely dynamically induced by climate changes in the stratosphere, the latter caused by stratospheric ozone depletion in the Arctic due possibly to increased halocarbon levels. To present our case, we analyze the daily data from the National Centers for Environmental Prediction/National Center for Atmospheric Research (NCEP/NCAR) reanalysis and simulation results from Goddard Institute for Space Studies'(GISS) GCM.

While high-latitude SATs show warming trends during the past few decades, the stratospheric Arctic polar vortex has been becoming colder and stronger (7 9) and persisting longer in springtime (10,11). Especially during 1990s there were fewer stratospheric major warmings, and total column ozone in the Arctic rapidly decreased and reached record low levels in the spring of 1997 (12). Late winter and early spring (February-March, FM) is the time when sunlight returns to the North pole and stratospheric Arctic ozone is chemically depleted. Though ozone depletion in the Arctic is not as severe as that in the Antarctic, satellite observations show that Arctic ozone has systematically declined since 1979. Because stratospheric temperature is very sensitive to the concentration of ozone, which is a good absorber of ultraviolet radiation, lowering ozone amounts have led to a strong cooling trend in the Arctic in late winter and early spring since 1979. Figure 1a shows a plot of March-mean total column ozone over 1979-2002, together with March-mean polar temperature anomalies over 1958-2002. Before 1979, ozone data is not available, and the polar temperature increased during the 1970s.

After 1979, both total column ozone and temperatures show systematic decreases, accelerating in the 1990s. Though mid-latitude ozone and temperatures have also decreased during the period 1979-2002 (7), their rates are much weaker than that in the Arctic. As a result, meridional temperature gradients between the Arctic polar region and middle latitudes are enhanced. This can be seen in Figure 1b which shows FM temperatures at 30 mb at middle latitudes and in the Arctic and their trends. The cooling trend in the Arctic is -0.25 K/yr, twice as large as the mid-latitude cooling trend, -0.11 K/yr. Thus, a temperature difference of about 3.4 K has developed over the past 24 years.

To illustrate meridional temperature differences at other levels and to compare them with those in early winter (November-December, ND), we plot 24-year trends in zonal mean temperatures for FM and ND in Figure 1c and d, respectively. For FM, it is found that at all stratospheric levels cooling in the Arctic is much stronger than that at middle latitudes (significance levels for the trends in the Arctic are generally above 90%). Weak trends with opposite signs are found in the upper troposphere around $60°$N, with warming in lower latitudes and cooling in high latitudes, suggesting a enhanced temperature gradient there. This could be a result of the greenhouse effect. However, it is weak and less significant. In contrast to the strong Arctic cooling in FM, high-latitude temperatures in ND exhibit weak warming in both the stratosphere and the troposphere. Therefore, results in Figure 1 state that enhanced temperature gradients happen only in late winter and springtime, and after 1979, suggesting that the stratospheric cooling should be a result of Arctic ozone depletion.

From the thermal wind relation, the enhanced temperature gradients must lead to stronger westerly zonal winds in the subpolar stratosphere. Data analysis has shown that subpolar stratospheric winds (located around $60°$N) have indeed increased by several ms^{-1} (3). Based on the linear wave theory (13, 14), the strengthened subpolar westerly winds should have the tendency to refract planetary waves away from the high latitudes, and the tendency can be characterized by the trends in the indices of refraction (The square of the index is used). Regions with negative trends tend to refract waves away, while regions with positive trends are the places where waves propagate toward. Figure 2a shows 24-year trends in wavenumber-1 refraction indices in FM. One can find that almost all the stratosphere is dominated by negative trends. A negative

band extends into the troposphere, with significance levels above 95%. A negative maximum is located in the upper troposphere between $50°$N and $60°$N. This is because the refraction index is very sensitive to changes of winds near the tropopause (15). Significant and positive trends are found in altitudes from about 5 km to 15 km and over $30°$N-$40°$N. In contrast, refraction indices show positive trends at high latitudes for ND, with weak negative trends at low latitudes (Figure 2b). Furthermore, a decrease of the index of refraction in FM is not found over 1958-1979 (Figure 2c). For ND, the refraction index does not exhibit a significant tendency over the 45 years (Figure 2d). The timing, with respect to the season and the decades, of the trend suggests that the significant changes in the index of refraction are associated with stratospheric Arctic ozone depletion.

Tendency of planetary wave propagation can be more explicitly demonstrated from the trends in Eliassen-Palm (E-P) flux vectors in Figure 3a and b (16). Downward arrows in Figure 3a means that over the 24 years upward wave propagation has been suppressed in JFM, due to a reduced upward E-P flux component. It is important to note that this reduction occurs at all levels in high latitudes. Equatorward arrows in the low-latitude upper troposphere means that more wave activity are refracted toward low latitudes due to increased equatorward horizontal E-P flux component. E-P flux vector trends for ND are generally upward and poleward (Figure 3b), reflecting nearly opposite tendencies of wave propagation between early and late winter. This is consistent with the refraction index trends in Figure 2a and b.

The background color shading in Figure 3a and b marks the trends in E-P flux divergence. According to the theory of wave-mean flow interactions (14), regions with negative trends in E-P flux divergence are the places where westerly zonal winds are weakened, while regions with positive trends are the places where westerly zonal winds are strengthened. In Figure 3a, the positive maximum in the subpolar stratosphere is indicative of strengthened polar night jet, while the negative maximum suggests that waves are more focused toward the tropospheric subtropics due to strengthened winds at high latitudes. The situation in ND is almost opposite, with positive trends in the upper troposphere between $30°$N and $60°$N and negative trends at high latitudes extending from the stratosphere to the troposphere.

To compare the 24-year trends with that over previous decades, we plot total vertical E-P

fluxes at 30 mb and 850 mb for JFM as a function of years in Figure 3c and e, respectively. At 30 mb, the total vertical E-P flux first increases over 1958-1979, then exhibits a significant downward trend over 1979-2002. At 850 mb, the E-P flux systematically declined since 1979. It is important to note that the decadal variation of E-P fluxes closely followed that of Arctic ozone. Both slowly decreased during the 1980s and then decreased more rapidly during the 1990s. For ND, the total vertical E-P flux at 30 mb shows significant increases over 1978-2001 (Figure 3d), and the E-P flux at 850 mb has no significant change over the 45 years. Our other calculations show that total vertical E-P fluxes at other levels all have the same tendencies as that at 30 and 850 mb (figures not presented here). These results here are consistent with other results concerning planetary wave activity in the stratosphere (18- 20) using different reanalysis data.

Reduced vertical E-P fluxes at all the levels are either a result of less wave activity generation in the troposphere or due to equatorward wave refraction or by their combination. To clarify this, we evaluated the E-P flux budget within the region between 850 and 30 mb and between $40°$N-$90°$N. Over 1979-2002, the reduction of total vertical E-P flux at 30 mb is $\delta F_{30mb} \approx -0.6 \times 10^{11} kgs^{-2}$, about 21% of that in 1979, and the reduction at 850 mb is $\delta F_{850mb} \approx -3.8 \times 10^{11} kgs^{-2}$, about 12% of that in 1979. Thus, the difference in upward E-P flux reduction between the two levels is $\delta F_z = \delta F_{30mb} - \delta F_{850mb} \approx 3.2 \times 10^{11} kgs^{-2}$. It approximates the 24-year increase of total horizontal E-P flux crossing $40°$N, $\delta F_{40°N} \approx -3.2 \times 10^{11} kgs^{-2}$ (note that the negative sign means that equatorward horizontal E-P flux is increased). This tells us that the reduction in vertical E-P fluxes is mostly due to equatorward wave refraction. Total horizontal E-P fluxes in JFM and ND are plotted in Figure 3g and h, respectively. The horizontal E-P flux in JFM exhibits a significant trend over 1979-2002 and no significant change over 1958-1979. This explain why there is a negative maximum in the low-latitude upper troposphere in Figure 3b. The total horizontal E-P flux in ND maintains no trend over the 45 years.

We emphasize three points in summarizing the observational analysis. First, decadally decreasing upward E-P flux is found only in JFM, which approximately matches the season of rapid ozone depletion in the Arctic. Second, the negative trend in upward E-P flux started

from 1979, which is the time when systematic ozone depletion began to take place in both poles. Third, upward E-P flux reduction at high latitudes occurs not only in the stratosphere, but extends to near the surface. It is the reduced wave activity near the surface that leaves more prevailing westerly winds associated with the AO over the high-latitude surface, which causes warming over the continents.

There are other possible external forcings in the atmosphere, such as increasing greenhouse gases and volcanic aerosols, which may also cause decreasing planetary wave activity through the same mechanism, i.e., enhancing meridional temperature gradients (21- 28). Can ozone depletion alone induce high-latitude SAT warming? This is further tested using GISS' GCM, with an ozone chemistry scheme that can generate ozone depletion comparable to the observed ozone depletion levels (28). Figure 4 shows 10-year (1990-1999) trends from the simulations. In the stratosphere, the trends in FM geopotential heights at 30 mb show a seesaw pattern similar to the NAM in the NCEP/NCAR reanalysis (34), with negative trends over the Arctic and a positive annular-like band over mid-latitudes. The magnitudes of the trends are found to be comparable to observations. At the surface, the spatial pattern of the trends in sea-level pressure (SLP) and SAT are also reasonably similar to that from observations (3). One can see warming trends over the high-latitude Europe-Asia continent and the western-part of the North American continent. Coolings are found over Aleutian and the region from the east coast of North America to Greenland. The magnitudes of the simulated SLP trends are close to the March-April observations, while the magnitudes of the simulated SAT trends seem to be weaker than observations. In an earlier simulation study using the same GCM (28), it was reported that the effect of ozone depletion is significant over March-April, though it is weak when averaged over the whole cold season (November-April).

That ozone depletion can induce surface climate change was previously reported in other GCM simulations (30), in which abnormal warming over the Northern-Hemisphere high latitudes during 1989-1994 was reproduced as observed ozone depletion over the same period was imposed in the GCM. A recent simulation work suggested that the European little ice age during the Maunder Minimum might be caused by decreased lower-stratospheric ozone in extra-polar region due to a weak reduction of solar emission during that period (31). In

that case, decreasing ozone in the extra-polar region led to weakened meridional temperature gradient and thus decreased planetary wave activity, which decelerated surface westerly winds over North Atlantic and consequently reduced transport of warm oceanic air to the European continent.

It has become a public concern that stratospheric ozone depletion can cause increasing solar ultraviolet radiation on the surface. In this study, we presented evidence showing that stratospheric ozone depletion can also dynamically induce surface climate change. The dynamic capability of ozone depletion is due to several reasons. First, ozone is a primary absorber of solar ultraviolet radiation. Stratospheric temperature is thus very sensitive to changes in stratospheric ozone mixing ratio. Arctic ozone depletion in late winter and springtime is so rapid and strong that it can cause significant changes in temperature gradients between the Arctic and middle latitudes. Then, the downward ozone trend induced significant enhanced subpolar temperature gradients. It is the enhanced temperature gradients that lead to significant dynamic impact on high-latitude surface climate change. Second, the dynamic impact of stratospheric ozone depletion on surface climate change is not through direct driving of the troposphere by the stratosphere, but through altering upward planetary wave propagation generated in the troposphere. An earlier study has first proposed an interpretation linking the Antarctic ozone hole with observed warming over the Antarctic Peninsula and the retreats of ice shelves there and suggested that the cause of high-latitude surface warming might initially arise from the stratosphere rather than from the troposphere (35). It also pointed out that the dynamical linkage of climate changes between the stratosphere and the troposphere is through changes in planetary wave activity, although diagnostics of the proposed links were not presented because of very limited observational data in the Southern-Hemisphere. Recent studies have provided more and more evidence indicating that the stratosphere can dynamically influence the troposphere and surface climate (21, 22, 29, 32- 34). Third, positive feedbacks amplifies the dynamic impact of ozone depletion on surface climate change. As wave activity was initially reduced due to ozone depletion, it caused less poleward ozone transport (20) and decreased wave-driven dynamical heating in the Arctic (19, 36). This positively feeds back to the original radiative change to cause a much colder and stronger polar vortex, which leads to more wave activity reduction.

References and Notes

1. Folland, C. K., T. R. Karl and K. Y. Vinnikov, *Climate Change, The IPPC Scientific Assessment*, ed. J. T. Houghton, Cambridge Univ. Press, Cambridge, U.K., 195 (1990).

2. Hurrell, M., *Science* **269**, 676 (1995).

3. Thompson, D. W. J., J. M. Wallace, and G. C. Hegerl, *J. Climate* **13**, 1018 (2000).

4. Thompson, D. W. J., and J. M. Wallace, *Geophys. Res. Lett.* **25,** 1297 (1998).

5. Hartmann, D. L., J. M. Wallace, V. Limpasuvan, D. W. J. Thompson, and J. R. Holton, *Proc. Nat. Acad. Sci.* **97**, 1412 (2000). This survey reviewed recent results on the NAM studies, interpreted dynamical connection of interannual climate variabilities between the troposphere and the stratosphere, and proposed possible external forcings that lead to the NAM index trend and relevant climate changes.

6. Wallace, J. M., and D.W.J. Thompson, *Physics Today* **55**, 29 (2002).

7. Randel, W. J., and F. Wu, *J. Climate* **12,** 1467 (1999).

8. Waugh, D. W., and W. J. Randel, *J. Atmos. Sci.* **56,** 1594 (1999).

9. Pawson, S., B. Naujokat, *J. Geophys. Res.* **104**, 14209 (1999).

10. Newman, P. A., J. F. Gleason, R. D. McPeters, and R. S. Stolarski, *Geophys. Res. Lett.* **24**, (1997).

11. Waugh, D. W., W. J. Randel, S. Pawson. P. A. Newman, and E. R. Nash, *J. Geophys. Res.*, **104,** 27191 (1999).

12. Scientific assessment of ozone depletion: 1998, Global Ozone Research and Monitoring Project. Rep. 37, World Meteorological Organization (1999).

13. Charney, J. G., and P. G. Drazin, *J. Geophys. Res.* **66**, 83 (1961).

14. Andrews, D. G., J. R. Holton, and C. B. Leovy, *Middle Atmosphere Dynamics*, Academic Press, New York, p. 489 (1987). From this text book, readers can find detailed physical

interpretation on the notations involved in the present article, such as the refraction index, vertical planetary-wave propagation, non-acceleration theorem, and wave-mean flow interaction.

15. Chen, P. and W. A. Robinson, *J. Atmos. Sci.* **51,** 2533 (1992).

16. In this study, E-P fluxes are three-month (January-February-March, JFM) average. Because of the long period of stratospheric vacillation (about two or three month, (17)), shorter-time averages yield non-significant trends due to too large fluctuations. It is noticed that January-mean E-P fluxes also show decreasing since 1979. However, this should not be the reason for obtaining the significant trend in JFM E-P fluxes, because NDJ E-P fluxes do not exhibit a significant trend (19).

17. Holton, J., and C. Mass, *J. Atmos. Sci.* **33**, 2218 (1976).

18. Zhou, S., A. Miller, J. Wang, and J. K. Angell, *Geophy. Res. Lett.* **28**, 4107 (2001).

19. Hu, Y., and K. Tung, *J. Climate* **15**, 1659 (2002).

20. Randel, W. J., F. Wu, and R. Stolarski, *J. Meteorol. Soc. Japan*, submitted (2002). In this article, the authors used data sets from NCEP/NCAR, European Center for Medium Range Weather Forecasts (ECMWF) and Climate Prediction Center (CPC) reanalyses. Results from the three data sets all show that over 1979-2002 vertical E-P fluxes have slight long-term increases in ND and significant decreases during JFM, with the largest decrease in February.

21. Rind, D., N. K. Balachandran, and R. Suozzo, *J. Climate*, **5,** 189 (1992).

22. Robock, A., and J. Mao, *Geophy. Res. Lett.*, **19**, 2405 (1992).

23. Graf, H.-K., I. Kirchner, A. Robock, and I. Schult, *Climate Dyn.* **9**, 81 (1993).

24. Rind, D., D. T. Shindell, P. Lonergan, and N. K. Balachandran, *J. Climate* **11,** 876 (1998).

25. Graf, H.-K., I. Kirchner, J. Perlwitz, *J. Geophys. Res.* **103**, 11251 (1998).

26. Shindell, D. T., D. Rind, P. Lonergan, *Nature*, **392**, 589 (1998).

27. Shindell, D. T., R. L. Miller, G. A. Schmidt, and L. Pandolfo, *Nature* **399**, 452 (1999).

28. Shindell, D. T., G. A. Schmidt, R. L. Miller, and D. Rind, *J. Geophys. Res.* **106**, 7193 (2001). The arcticle describes the model setup for carrying out the simulation results presented here.

29. Baldwin, M. P., and T. J. Dunkerton, *J. Geophys. Res.* **104**, 30937 (1999).

30. Volodin, E. M., and V. Ya. Galin, *J. Climate* **12**, 2947 (1999).

31. Shindell, D. T., G. A. Schmidt, M. E. Mann, D. Rind, and A. Waple, *Science* **294**, 2149 (2001).

32. Perlwitz, J., and H. F. Graf, *J. Climate* **8** 2281 (1995).

33. Kodera, K., and H. Koid, *J. Geophys. Res.* **102**, 19433 (1997).

34. Baldwin, M. P., and T. J. Dunkerton, *Science* **294**, 581 (2001).

35. Thompson, D. W. J., and S. Solomon, *Science* **296**, 895 (2002).

36. Newman, P. A., E. R. Nash, and J. E. Rosenfield, *J. Geophys. Res.*, **106**, 19,999 (2001).

37. We have benefited from discussion with Ron Miller and David Rind. The work at GISS/Columbia University is supported by NASA's Atmospheric Chemistry Modeling and Analysis Program and by NSF ATM-00-02267, and the work at University of Washington is supported by the National Science Foundation, Division of Atmospheric Sciences, Climate Dynamics, under grant ATM 9813770. NCEP Reanalysis data is provided by the NOAA-CIRES Climate Diagnostics Center, Boulder, Colorado, USA, from the Web site at http://www.cdc.noaa.gov/.

Figure captions

Figure 1: (a) March TOMS total column ozone (Dobson Units), area-weighted over $65°$N-$75°$N (solid line), against March temperature anomalies at 30 mb (dotted-line), area-weighted over $65°$N-$90°$N. For comparison, temperature anomaly, $T^{'}$, is re-scale by $3.0 \times T' + 430$K, (b) area-weighted FM mean temperatures over $40°$N-$60°$N (solid line) and $65°$N-$90°$N (dashed-dotted line), dashed and dotted lines are the trends in these temperatures, (c) 24-year (1979-2002) trends in FM zonal-mean temperatures. (d) 24-year (1978-2001) trends in ND zonal-mean temperatures. Black contours are student t-test values. Hereafter, t-test value 2 corresponds the significance level of about 95%.

Figure 2: Trends in wavenumber-1 refraction index square at 400 mb. (a) 24-year (1979-2002) trends for JFM, (b) 24-year (1978-2001) trends for ND. Balck contours in (a) and (b) are student's t-test values. The plots are limited between $30°$N and $70°$N to avoid extremely large fluctuations of n^2 near the critical layer and Arctic interior where the linear wave theory is invalid. (c) and (d) Wavenumber-1 refraction indices for FM and ND, respectively, averaged over $50°$N-$60°$N, as a function years. Here, n^2 is multiplied by earth's radius square, a^2.

Figure 3: (a) 24-year trends in E-P flux vectors (white arrows) and E-P flux divergence (color shading) in ND. Black contours mark t-test values for the trends in E-P flux divergence, and (b) same as (a) except for FM. The E-P flux vectors and the divergence field are divided by background air density to make them visible at high levels. The scaling vectors in (a) and (b) is $1.0 \times 10^(8) kgs^{-2}$. (c), (e), and (g) are respective plots of total vertical E-P flux crossing 30 mb and 850 mb, integrated over $40°$N-$90°$N, and total horizontal E-P flux crossing $40°$N, integrated from 1000 mb to 20 mb, in JFM. (d), (f), and (h) are same as (c), (e), and (f), respectively, except for ND.

Figure 4: 10-year simulation trends due to ozone depletion alone. Left: Trends in FM geopotential heights anomalies at 30 mb, middle: trends in sea-level pressure anomalies during March-April, and right: trends in SAT anomalies during March-April. The trends are calculated from two GCM runs. One run includes both ozone depletion and increasing greenhouse gases. The other one has increasing greenhouse gases only.

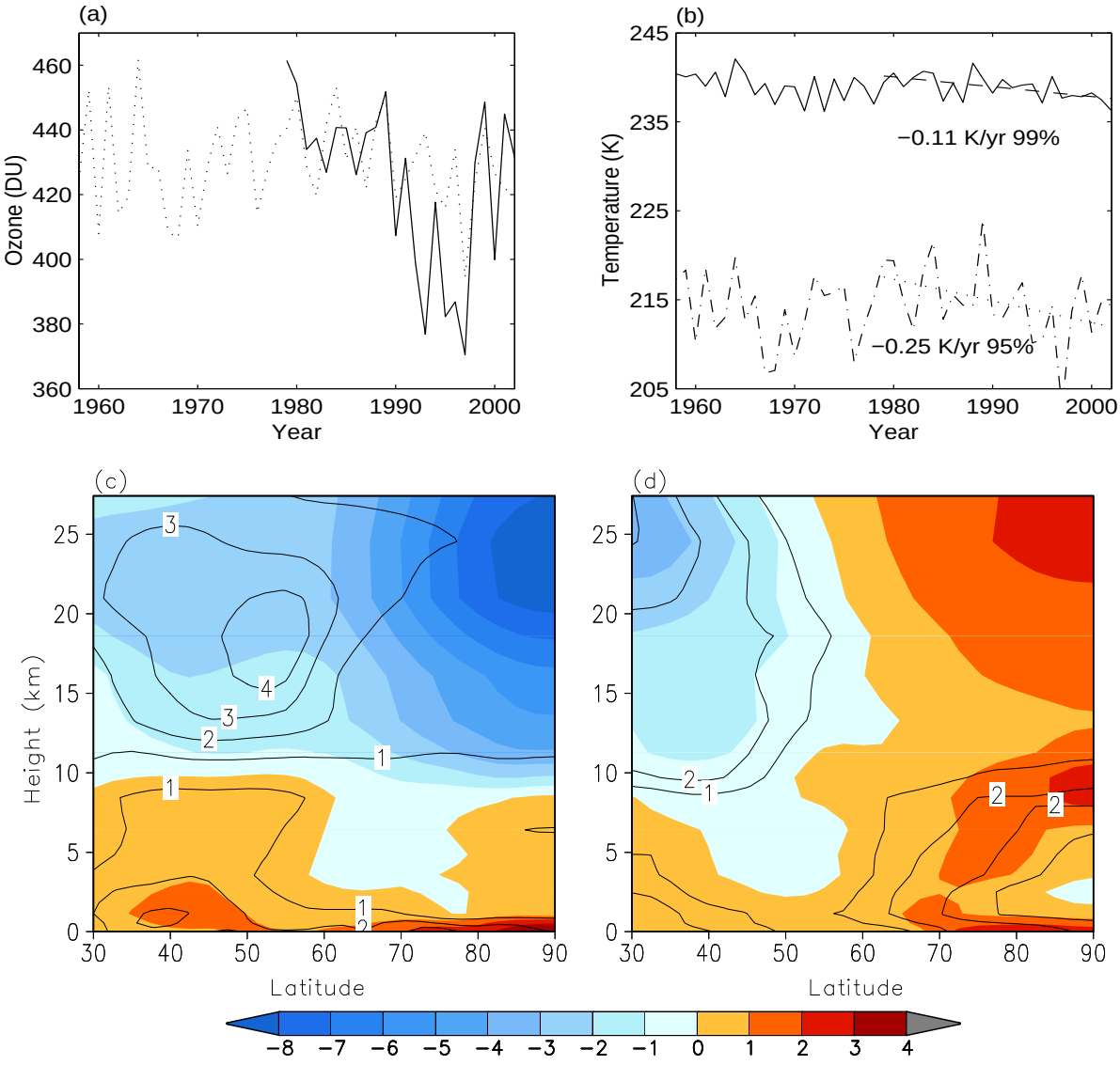
(a)
Ozone (DU)
460
440
420
400
380
360
1960
1970
1980
1990
2000
Year
(b)
Temperature (K)
245
235
225
215
205
−0.11 K/yr 99%
−0.25 K/yr 95%
1960
1970
1980
1990
2000
Year
(c)
(d)
Height (km)
25
20
15
10
5
0
30
40
50
60
70
80
90
Latitude
Latitude
−8
−7
−6
−5
−4
−3
−2
−1
0
1
2
3
4

Fig. 1.

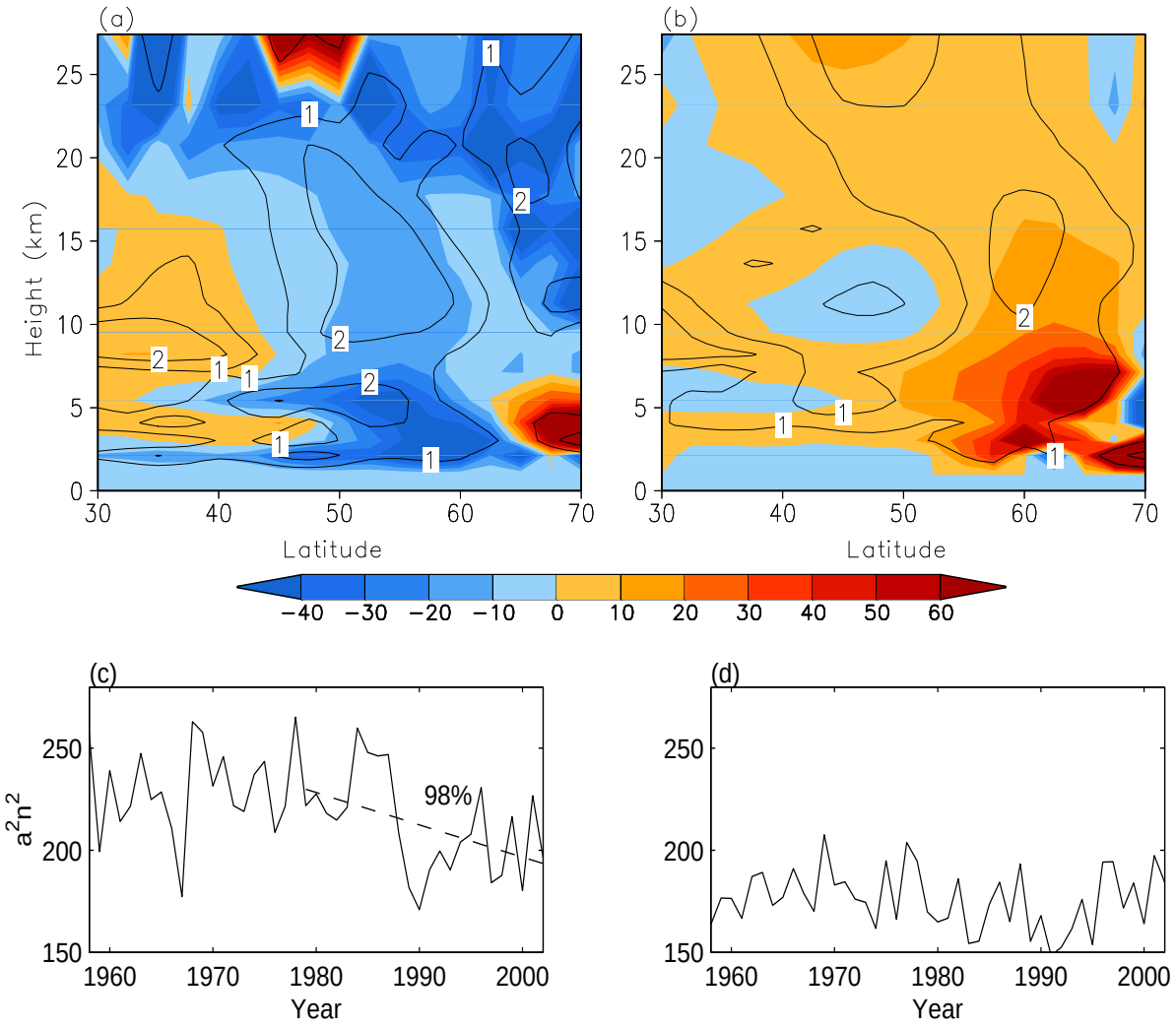
(a)
(b)
Height (km)
Latitude
Latitude
−40 −30 −20 −10 0 10 20 30 40 50 60
(c)
(d)
98%
a^2n^2
Year
Year

Fig. 2.

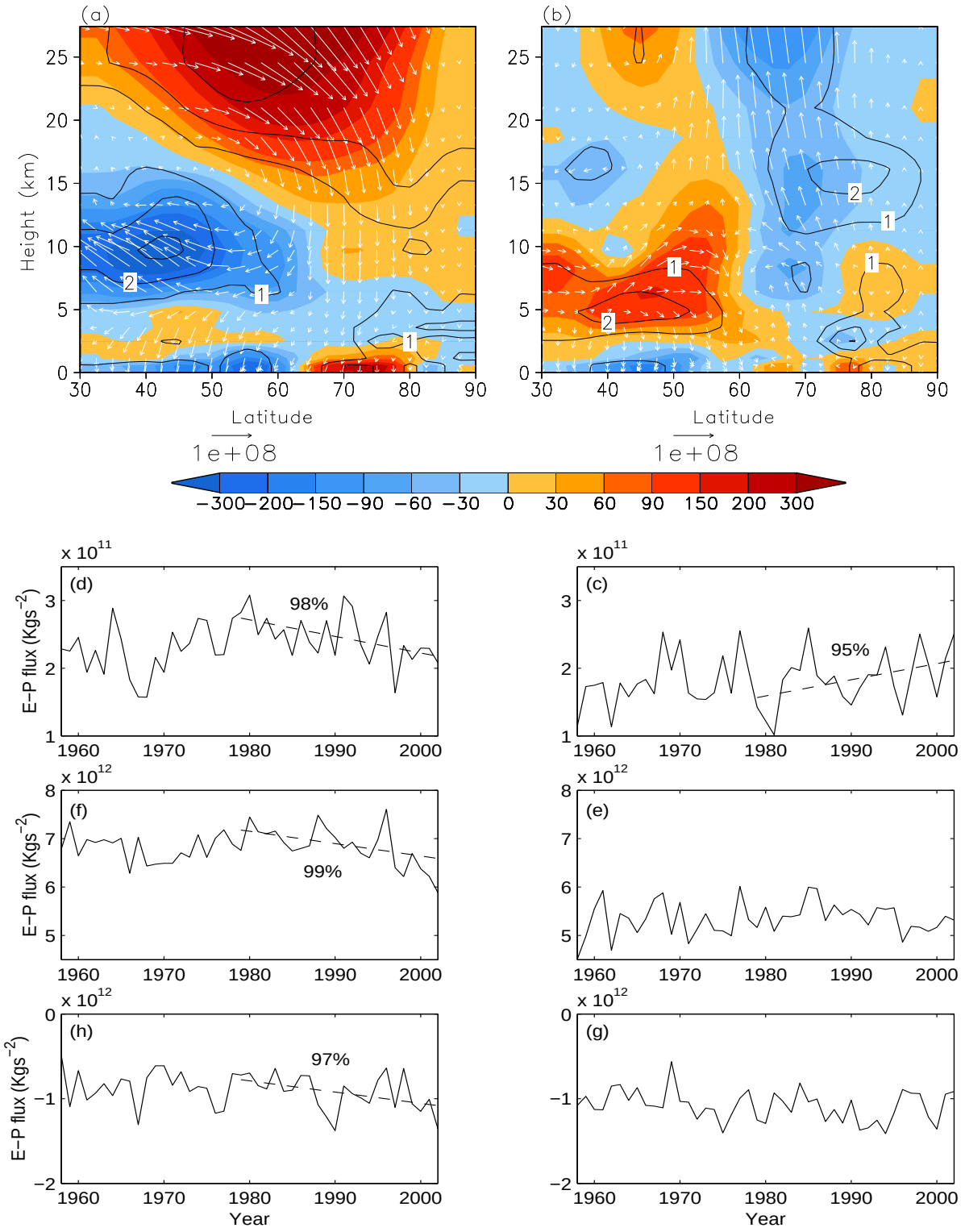
(a)
(b)
Height (km)
Latitude
1e+08
−300 −200 −150 −90 −60 −30 0 30 60 90 150 200 300
(d)
98%
(c)
95%
(f)
99%
(e)
(h)
97%
(g)
E−P flux (Kgs^{-2})
x 10^{11}
x 10^{12}
Year

Fig. 3.

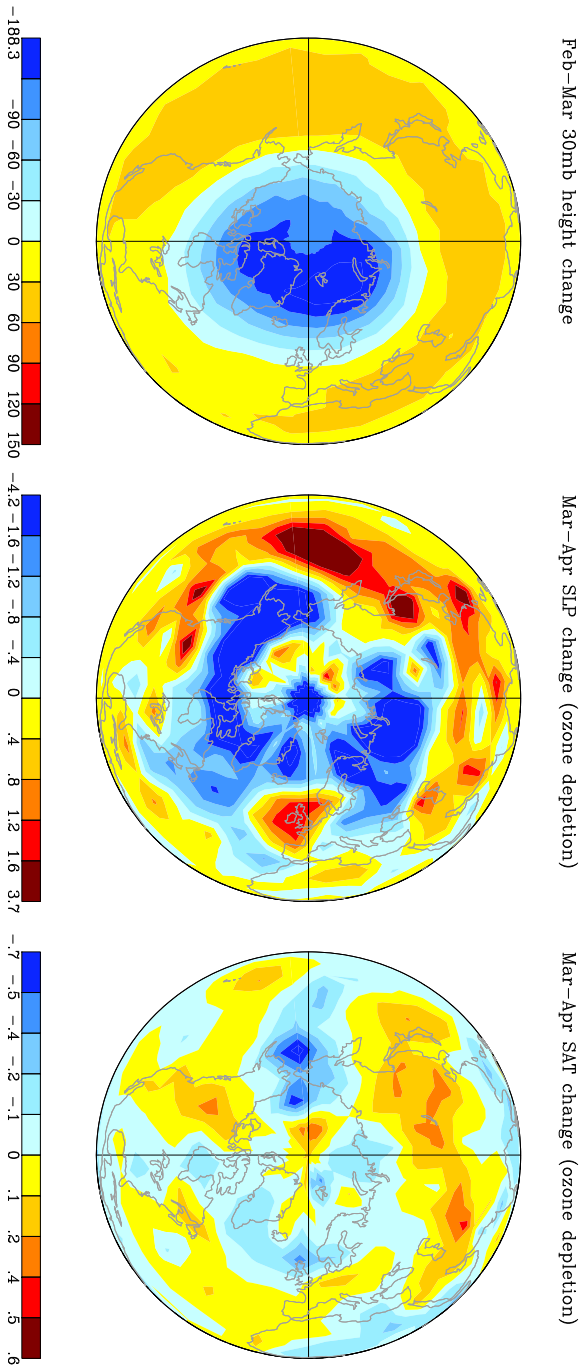
Feb–Mar 30mb height change
−188.3 −90 −60 −30 0 30 60 90 120 150
Mar–Apr SLP change (ozone depletion)
−4.2 −1.6 −1.2 −.8 −.4 0 .4 .8 1.2 1.6 3.7
Mar–Apr SAT change (ozone depletion)
−.7 −.5 −.4 −.2 −.1 0 .1 .2 .4 .5 .6

Fig. 4.